

Utilizing localized fast radio bursts to constrain their progenitors and the expansion history of the Universe

Sandeep Kumar Acharya,^{a,1} Paz Beniamini^{a,b,c}

^a*Astrophysics Research Center of the Open University, The Open University of Israel, Ra'anana, Israel*

^b*Department of Natural Sciences, The Open University of Israel, P.O Box 808, Ra'anana 4353701, Israel*

^c*Department of Physics, The George Washington University, 725 21st Street NW, Washington, DC 20052, USA*

E-mail: sandeepa@openu.ac.il

ABSTRACT: Fast radio bursts (FRBs) are increasingly being used for cosmological applications such as measuring the Hubble constant and baryon abundance. The increasing number of localized FRBs and precise measurement of dispersion measure (DM) make them a suitable probe for such an approach. We use a sample of 110 localized FRBs as well as a small sub-sample of 24 FRBs with scattering timescale measurements or limits. We infer the Hubble constant (H_0) and the DM distribution of the host galaxies simultaneously by fitting our model to the FRB DM measurements. With current data, our results are in agreement with both high and low redshift measurements of H_0 , obtained using Cosmic Microwave Background (CMB) and Type Ia supernovae data respectively. We project that with about 200 localized FRBs, we would be in a position to distinguish between the two scenarios at 4σ confidence. In addition, the host DM is expected to be related to star formation in the host galaxy and the stellar age of the progenitors. Using our inferred host galaxy DMs, we are able to rule out (at 95 percent confidence) a majority of localized FRB progenitors originating from young sources with stellar ages less than 10 Myr. This might reflect a large population of old sources or an observational bias against detecting FRBs from young sources, which may be associated with long scatter broadening times and large DM from their source environments. Indeed, we find that scatter broadening times of FRBs are inconsistent with the Milky Way ISM, but at the same time, do not appear to be strongly correlated with the FRBs' redshift or with the SFR or stellar mass of their host galaxies. This suggests that scattering is dominated by the immediate environment of the sources.

¹Corresponding author.

1 Introduction

Fast radio bursts (FRBs) are millisecond duration cosmological transients and have so far been observed in the frequency range of 100 MHz- 8 GHz. Till date, over 100 FRBs have been localized to their host galaxies (e.g. [1–3]). An important observable of a FRB is its dispersion measure (DM) which is the line of sight integral of electron density as the radio waves travel through the ionized medium. The observed DM of FRBs are measured very precisely. For typical values of DM of the order of few 100 - 1000 pc cm⁻³, the error is of the order O(1) pc cm⁻³ or less. Some of these FRBs have additional data on scattering timescales which captures broadening of the radio pulses. The observed DM is a combination of the intergalactic medium (IGM) or a cosmological component, a galactic and halo contribution from our own galaxy as well as the host galaxy contribution. The IGM DM captures relevant information for cosmological applications. Such applications include determining the baryon contents in the Universe, measuring the Hubble constant and probing the era of reionization etc [1, 2, 4–16].

The Hubble tension has been a matter of intense interest over the last few years. The inferred Hubble constant (H_0) from high z probes such as the CMB [17] is apparently at a 4σ tension with low z direct measurements of Type Ia supernovae [18] (see [19] and references therein for more details). FRBs provide an independent way to infer the constant and have already been used to determine H_0 [1, 9, 20–25]. The IGM DM provides us with a handle on the distance to FRBs, provided we know the average electron density in the universe. In addition, localization of a FRB host galaxy gives us the object’s redshift. The distance vs redshift relation provides us with the measurement of H_0 . Since the electron density fluctuates along different lines of sight, this measurement is noisy. Therefore, with the currently moderately sized sample of localized FRBs, one cannot statistically distinguish between the high redshift and low redshift H_0 . However, the number of localized FRBs is increasing rapidly. High precision H_0 determination using FRBs should be possible within a few years.

From the available DM data, one can infer the average host DM, even though the host contribution to the total DM for a given FRB is uncertain. From the point of view of using FRBs as a cosmological tool, the host DM adds noise to the determination of H_0 from FRB data. That being said the host DM and its evolution with other host galaxy properties carries vital information for our understanding of FRB sources (see e.g. [26]). Both zoom-in galaxy simulations [10, 27] and observations of Galactic pulsars and magnetars (as discussed in this work) find that host DMs vary as a function of stellar age. Therefore the average age of FRB progenitors can be constrained by extracting the host DM contribution from the data, informing us about FRB formation channels. A younger average source age, would suggest that FRBs track the star formation rate, as expected for magnetars formed via core-collapse supernovae (CCSNe) while older ages hint at alternate FRB formation channels.

Clearly, the use of FRBs as cosmological tools is coupled with the understanding of their progenitor contributions. In order to extract the IGM component, one has to marginalize over the apriori uncertain host and halo contributions. The host galaxy DM, along with scattering timescale measurements constrain the FRBs’ source environment and the typical age of their progenitors. In this work, we infer the rate of expansion of the Universe or Hubble constant as well as the age of FRB progenitors from a sample of localized FRBs simultaneously, by fitting our model to the available data. We use a

sample of 110 FRBs in this paper (Sec. 2). Inferring H_0 requires modeling the variation of DM_{IGM} across different sightlines and redshifts. This is provided by cosmological simulations. Almost all the works in the literature use the Illustris [28] simulation. In this work, we use the Cosmic Dawn II [29] simulation as our fiducial case (Sec. 3). We find that both simulations provide similar results using current data. The inferred H_0 value is consistent with both low and high z measurements within 1σ confidence (Sec. 5). We project that with about 200 FRBs, we should be in a position to distinguish the two scenarios at $\gtrsim 4\sigma$ confidence (Sec. 6). Though this result, in principle, depends somewhat on the redshift distribution of FRBs, it does not change the quantitative results substantially. Further, by comparing our obtained constraint on host DM to the observed DM of Galactic pulsars as a function of their spindown age, we are able to constrain the age of FRB progenitors assuming the pulsar spindown time is a proxy of stellar age. Assuming a single log-normal distribution of host DMs, we are able to rule out a majority of progenitors with an age younger than 10 Myr at 95 percent confidence interval (Sec. 7). In Sec. 8, we use the scattering timescale of a small sample of FRBs to study their correlation with host DMs as well as any information they may carry about their progenitors. Most of the host galaxies in this sample are starforming and, therefore, we need a bigger sample with more quiescent galaxies to test any potential correlation. We finish with our conclusions in Sec. 9.

2 Sample of FRBs used in this work

The observed dispersion measure of FRBs can be partitioned to its individual components as,

$$DM_{\text{obs}} = DM_{\text{halo}} + DM_{\text{ISM}} + DM_{\text{IGM}} + \frac{DM_{\text{host}} + DM_{\text{source}}}{1 + z} \quad (2.1)$$

where DM_{ISM} and DM_{halo} are the contributions due to our own galaxy and its circumgalactic medium. The cosmological component, DM_{IGM} , is contributed by the large scale structure of the universe. It depends sensitively on the evolution of these structures and, therefore, on the expansion history of the universe. DM_{host} and DM_{source} are due to the host galaxy of the FRB and the immediate surrounding of the FRB respectively which are redshifted to the observer frame. Currently, the host and halo contribution have the largest level of uncertainty. In this work, we used $DM_{\text{halo}} = 50 \text{ pc cm}^{-3}$ as our fiducial value which is in agreement with recent works [1] (furthermore it is likely an overestimate and thus a conservative choice in this context)¹. We compute the ISM contribution using two available models in the literature, NE2001 [31] and YMW2017 [32]. We use NE2001 as our fiducial model unless otherwise stated. In order to minimize the source contribution we drop 20121102A and 20190520B from our sample while using their DM as the observable. However, we include them in our scattering timescale sample (Sec. 8). These sources are likely young, as evidenced by their large rotation measures [33, 34] and persistent radio emission [35, 36]. Thereby, by removing these sources we ensure minimal contamination due to source terms, if any. In Table 2, we show our sample of 110 localized FRBs along with their observed redshift, total DM, galactic contribution alongside the references. In Sec. A, we plot the observed DM of our sample of FRBs after subtracting their ISM and halo contribution and compare them with the expected DM from IGM within our fiducial cosmological model. We explain this further in subsequent sections.

¹However, the halo contribution may be anisotropic according, see [30].

3 Dispersion measure

3.1 DM_{IGM}

The expression for mean IGM contribution can be written as [10],

$$\langle DM_{\text{IGM}}(z) \rangle = \frac{3cH_0\Omega_{\text{b}0}}{8\pi Gm_{\text{p}}} \int_0^z dz' \frac{(1+z)\xi_e(z)}{[\Omega_{\text{m}0}(1+z')^3 + \Omega_{\Lambda 0}]^{1/2}} \quad (3.1)$$

where $\langle DM_{\text{IGM}}(z) \rangle$ is the average contribution and is a function of z (for a given set of cosmological parameters), averaged over different line of sight directions. The parameters $\Omega_{\text{b}0}$, $\Omega_{\text{m}0}$ and $\Omega_{\Lambda 0}$ are the fractional energy density of baryons, matter and dark energy compared to the critical energy density today which capture the expansion history of the universe. In a flat Λ CDM universe, $\Omega_{\Lambda 0} = 1 - \Omega_{\text{m}0}$. We use the best fit value of these parameters as inferred from the CMB (Cosmic Microwave Background) experiments [17]. The dispersion measure is a function of the free electron abundance which is captured by $\xi_e(z)$, which in turn depends upon the helium mass fraction (Y). At $z \lesssim 3$, helium is fully ionized. Therefore, using $Y \approx 0.25$, we have $\xi_e(z) \approx 0.87$.

From Eq. 3.1, we find that $\langle DM_{\text{IGM}}(z) \rangle \propto \Omega_{\text{b}0}H_0$. The degeneracy between $\Omega_{\text{b}0}$ and H_0 can be broken by using independent measurement such as from CMB (Cosmic Microwave Background) experiments [17]. CMB primary anisotropy measurement constrain $\Omega_{\text{b}0}h^2$ very precisely where $H_0 = 100h \text{ kms}^{-1}\text{Mpc}^{-1}$. From *Planck* measurements, we have, $\Omega_{\text{b}0}h^2 = 0.02242 \pm 0.00014$ [17]. For the current expected level of precision from FRB data, we can use the mean value of $\Omega_{\text{b}0}h^2$ to break this degeneracy. In that case, DM_{IGM} is inversely proportional to h [12]. We take our fiducial value of h to be 0.7. Therefore, the expression for mean IGM DM at a general h can be parameterized as,

$$\langle DM_{\text{IGM}}(z, h) \rangle = \langle DM_{\text{IGM}}(z, h = 0.7) \rangle \left(\frac{0.7}{h} \right) \quad (3.2)$$

The dispersion measure can have a significant scatter along different lines of sight due to fluctuation in matter density. This leads to a variance in the IGM contribution. This quantity is difficult to compute analytically and, therefore, cosmological simulations are used to infer this quantity. As can be expected, this variance can have a sensitive dependence on simulations due to their treatment of baryonic physics. We consider two such simulations below.

3.1.1 Cosmic Dawn (CoDa)

We choose our fiducial choice of cosmological simulation to be Coda II [29] which is a fully-coupled, large-scale, high-resolution, radiation-hydrodynamical simulation including galaxy formation and reionization up to redshift $z \approx 5.8$. At lower redshifts, the universe is ionized, therefore, the ionization field mimics the matter field. The authors in [37] do a dark matter only, N-body simulation (called "Coda II Dark matter" simulation) to extend the results to $z = 0$. These simulations are run on same initial conditions as Coda II. The authors parameterize the standard deviation of $DM_{\text{IGM}}(z)$. For $z \lesssim 3$, the IGM dispersion measure can be parameterized as a lognormal distribution with mean as in Eq. 3.1 with $\sigma_{\text{IGM}}(z)$ as,

$$\sigma_{\text{IGM}}(z) = \sinh^{-1}(0.316z^{-0.677}). \quad (3.3)$$

We assume this relation to be valid for our fiducial case with $h = 0.7$. For different h , one needs to redo the simulations. However, since $\sigma_{\text{IGM}}(z)$ is the variance of a lognormal distribution of DM_{IGM} (or $\frac{\text{DM}_{\text{IGM}}}{\langle \text{DM}_{\text{IGM}} \rangle}$), we do not expect a strong h dependence. Therefore, we use Eq. 3.3 as the expression for $\sigma_{\text{IGM}}(z)$ without having any dependence on h .

3.1.2 IllustrisTNG

We use IllustrisTNG [28] as our alternate choice of simulation. Similar to CoDa, it is a large scale gravity+magnetohydrodynamical simulation. The TNG suites include updates to galaxy formation models as well as other technical details which the reader can find in the reference. The host galaxy DM distribution is fitted with the expression [9, 38],

$$\frac{dp_{\text{IGM}}}{d\text{DM}_{\text{IGM}}} = A\Delta^{-\tilde{\beta}} \exp\left[-\frac{(\Delta^{-\tilde{\alpha}} - C_0)^2}{2\tilde{\alpha}^2\sigma^2}\right] \quad (3.4)$$

where $\Delta = \frac{\text{DM}_{\text{IGM}}}{\langle \text{DM}_{\text{IGM}} \rangle}$, $\tilde{\alpha} = \tilde{\beta} = 3$ and the fitting values of A , C_0 and σ are provided in [38]. Converting the variable from DM_{IGM} to $\log(\text{DM}_{\text{IGM}})$, we have the equivalent expression,

$$\frac{dp_{\text{IGM}}}{d\log(\text{DM}_{\text{IGM}})} = A \times \text{DM}_{\text{IGM}} \times \Delta^{-\tilde{\beta}} \exp\left[-\frac{(\Delta^{-\tilde{\alpha}} - C_0)^2}{2\tilde{\alpha}^2\sigma^2}\right], \quad (3.5)$$

The factor Δ has the dependence on $\langle \text{DM}_{\text{IGM}} \rangle$ which makes it a variable in terms of h using Eq. 3.2. We note that the fitting function A , C_0 and σ can have a dependence on h as well but we need to simulate these cosmologies in order to get their correct values. In this work, we take the simplifying assumption of these fitting function to be independent of h .

3.2 DM_{host}

We initially assume the host contribution to be lognormal as is standard in the literature [9] and consistent with numerical simulations [27]. We denote the mean value of the lognormal distribution as μ . The variance is denoted as σ_{host} . We assume the fiducial value of $\sigma_{\text{host}}=1$ which is roughly the average value obtained from simulations (Table 2 of [27]). Additionally, DM_{host} (in the rest frame) may be z dependent. This can be parameterized as $\text{DM}_{\text{host}} = \text{DM}_{\text{host},0}(1+z)^\alpha$. As an example, the authors of [39] reported an approximate value of $\alpha \approx 1$, on average across all galaxy types, using IllustrisTNG simulation[40]. However, current data can only exclude the scenarios with $|\alpha| \gtrsim 2$ at 68 percent confidence [26]. Therefore, in this work, we assume that host galaxy contribution does not evolve with redshift and $\alpha = 0$. We denote $\mu_0 \equiv \mu(z = 0)$, since our canonical model assumes $\alpha = 0$, μ can be replaced with μ_0 in the rest of the paper.

4 Likelihood evaluation

We use Gaussian likelihood for the data analysis. The likelihood of a given FRB with total observed DM ($\text{DM}_{i,\text{obs}}$) is given by,

$$\mathcal{L}_i(\text{DM}'_i|z_i) = \int_0^{\text{DM}'_i} \frac{dp_{\text{host}}(\text{DM}_{\text{host}}|\mu_0, \sigma_{\text{host}})}{d\text{DM}_{\text{host}}} \frac{dp_{\text{IGM}}(h)}{d\log X} d\text{DM}_{\text{host}}, \quad (4.1)$$

where, $DM'_i = DM_{i,\text{obs}} - DM_{i,\text{ISM}} - DM_{\text{halo}}$ and $X = DM'_i - \frac{DM_{\text{host}}}{1+z_i}$. The distribution of host galaxy DMs is given by,

$$\frac{dp_{\text{host}}}{dDM_{\text{host}}} = \frac{1}{\sqrt{2\pi\sigma_{\text{host}}^2} DM_{\text{host}}} \exp\left(-\frac{(\log(DM_{\text{host}}) - \mu_0)^2}{2\sigma_{\text{host}}^2}\right), \quad (4.2)$$

For results related to CoDa II simulation, we have the IGM distribution as,

$$\frac{dp_{\text{IGM}}(h)}{d\log X} = \frac{1}{\sqrt{2\pi\sigma_{\text{IGM}}^2}} \exp\left(-\frac{[\log X - \log(\langle DM_{\text{IGM}} \rangle)]^2}{2\sigma_{\text{IGM}}^2}\right), \quad (4.3)$$

For results using IllustrisTNG simulation, we use Eq. 3.5 as the IGM probability distribution while replacing DM_{IGM} by X .

The computed likelihood is a function of two parameters h and μ_0 . The h dependence is included in $\langle DM_{\text{IGM}}(z, h) \rangle$. Since all FRB sources are independent, the joint likelihood is given by the individual likelihood products,

$$\mathcal{L}_{\text{tot}} = \prod_i^N \mathcal{L}_i, \quad (4.4)$$

where N is the number of FRBs in the sample which is 110 in our case. We use MCMC (Markov Chain Monte Carlo) sampling to scan over the parameter space.

5 Dependence of H_0 determination on IGM and ISM modeling

We obtain marginalized constraints on h and μ_0 using the results of the two simulations that we have described before. We plot the constraints in Fig. 1. The constraint on h is $0.7^{+0.11}_{-0.07}$ and $0.64^{+0.11}_{-0.09}$ for IllustrisTNG and CoDa simulations respectively. They are consistent with each other as well with the result of [1] to within a 1σ confidence interval. The best fit value of $\mu_0 \approx 4$ applies to both cases. While our fiducial model above assumed NE2001 as the ISM model, we redo the same computation with the YMW2017 model. We obtain almost identical results. Therefore, we do not expect the choice of ISM model to affect the constraint in h .

6 Future projections on constraining h and viability of resolving Hubble tension

Our constraint on h is consistent with respect to high z probes such as the CMB [17] and low z probes such as Type Ia supernova [18] within 1σ confidence. The Hubble constant inferred from CMB observations ($H_0 = 67.4^{+0.5}_{-0.5}$ km s⁻¹Mpc⁻¹) is at $\approx 4\sigma$ tension with low redshift measurements ($H_0 = 74.0^{+1.4}_{-1.4}$ km s⁻¹ Mpc⁻¹). It is natural to ask if a larger FRB sample than what is available right now can distinguish between the two H_0 values at a high confidence interval. For this purpose, we do a simulation by generating a sample of FRBs with a redshift and DM_{host} distribution. We consider a universe with $h = 0.74$ which is what is measured from low redshift probes.

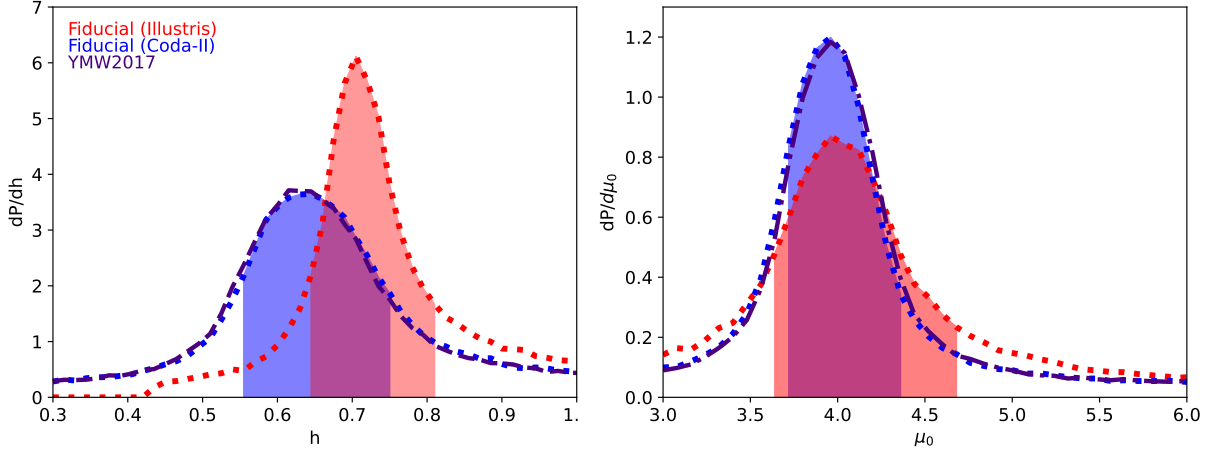


Figure 1: Marginalized probability distribution function for h and μ_0 by fitting these parameters to our sample of 110 FRBs. We show the 68 percent confidence interval in shaded regions for respective cases with the same color.

In Fig. 2, we plot the number of FRBs with known z (from the sample in Table 2) in redshift intervals of 0.1. We use an approximate normalized probability density function in Fig. 2 such that $\int_0^1 dz \frac{dP}{dz} = 1$. The rest frame host DM distribution is assumed to be lognormal with $\mu_0 = 4$ (best fit value in Fig. 1) and $\sigma_{\text{host}} = 1$ (see §3.2). We sample from a lognormal distribution of DM_{IGM} (with Eq. 3.2, 3.3 as the mean and variance respectively). At the sample creation stage, we assume the mean value of $\text{DM}_{\text{halo}} = 50 \text{ pc cm}^{-3}$ with a uniformly distributed scatter of up to $\pm 30 \text{ pc cm}^{-3}$. At the inference stage, we assume a constant $\text{DM}_{\text{halo}} = 50 \text{ pc cm}^{-3}$. For ISM contribution, we assume FRBs to be isotropically distributed in the sky but with positive declination angle. This is due to the sparsity of FRBs with negative declination angle in the current sample. For a given line of sight, we take the average of DM_{ISM} of the nearest 4 FRBs which encloses the simulated FRB in terms of sky location. We use the NE2001 model in the sample creation stage and use YMW2017 model in the inference stage. This procedure captures the uncertainty introduced due to our modeling choices.

We compute the likelihood of our simulated sample using the same formalism as in Sec. 4. We note that the likelihood is a function of two parameters h and μ . We marginalize over μ to compute the likelihood involving only h . We convert it into χ^2 distribution using the definition, $\chi^2(h) = -2 \times \log \mathcal{L}(h)$ where $\mathcal{L}(h)$ is the marginal likelihood over h . The absolute value of χ^2 is not physical. Therefore, We compute $\Delta \chi^2(h)$ by taking the minimum value of $\chi^2(h)$ distribution as zero. This quantity is plotted for a few cases in Fig. 3. We find that with our fiducial approximate distribution, ~ 200 FRBs would be enough to distinguish between the H_0 values reported by low and high redshift probes at 4σ confidence. The constraint is expected to be sensitive to the redshift distribution of FRBs. At high redshifts, the observed DM of FRBs is dominated by the IGM component and not polluted by the host contribution. Therefore, we expect to obtain stronger constraint on h compared to our fiducial case, assuming Λ CDM cosmological model. We simulate such a scenario with a uniform distribution

of FRBs over redshift range of 0 and 1. We also consider a more realistic case where the number of FRBs track the cosmic star formation rate (see [10, 41] for more details) and it is assumed that all FRBs are detected above a critical fluence threshold of 1 Jy ms at 0.5 GHz. Other relevant parameters can be found in Sec 2 of [10]. This calculation is representative of a hypothetical survey with good enough localization, such that a large fraction of detected FRBs can also be assigned a redshift (this is as opposed to the current sample of FRBs with z which is clearly biased towards low z - however note that planned surveys such as DSA 2000 [42] and CHORD [43] are expected to have \sim arcsec localization capabilities or better). For either of these redshift distributions, we find that we obtain stronger constraints than our fiducial case with 200 FRBs. In either case, we expect to distinguish between the two H_0 values with few hundred localized FRBs.

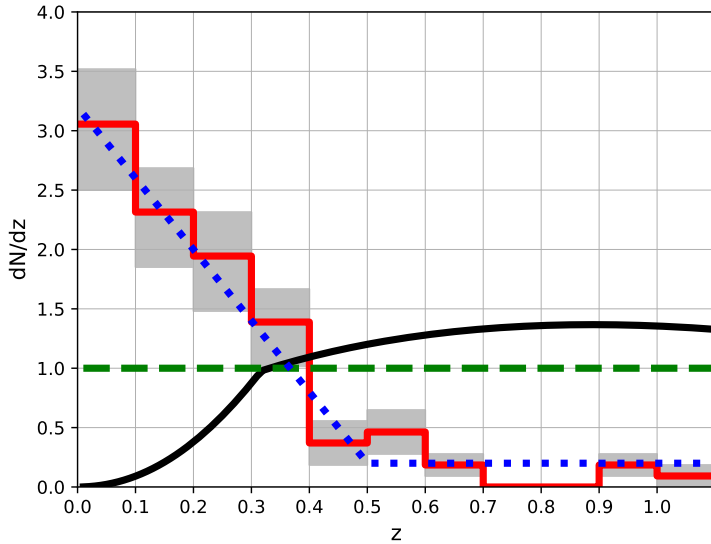


Figure 2: Normalized redshift distribution of the FRB sample. In red, we show the number of FRBs in Table 2 within $\Delta z = 0.1$ intervals along with the Poisson error in gray. The corresponding approximate distribution is shown in dotted blue. We also consider a uniform distribution (dashed green) between $z = 0 - 1.0$ and a more physically motivated distribution for a hypothetical future large FoV telescope with good localization capabilities (in black; see §6).

7 Constraining the age of FRB progenitors

Our inferred DM_{host} (Right panel of Fig. 1) have implications regarding the age of FRB progenitors. For young progenitors, which are likely to reside in regions of active star formation, we expect higher DM_{host} and the opposite at older ages. We empirically relate stellar age with DM_{host} , using the catalog of pulsars in our own galaxy². We use their tabulated spindown age as a proxy for stellar age. We

²<https://www.atnf.csiro.au/research/pulsar/psrcat/>

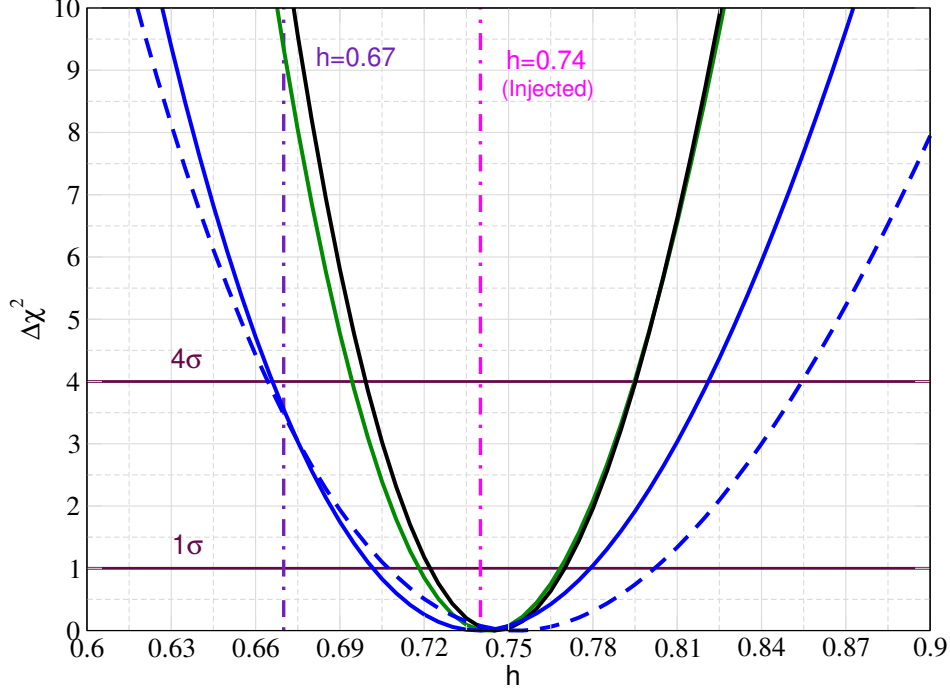


Figure 3: Futuristic constraints from an FRB sample of a given size (denoted in the plot). The color coding follows from Fig. 2. In dashed blue, we consider a scenario where half of total population of FRBs is contributed by young magnetars with $\langle DM_{\text{host}} \rangle \approx 350 \text{ pc cm}^{-3}$ (see Sec. 7 for details). In our simulation, we create a FRB sample with a background Hubble constant $h = 0.74$. We use 200 FRBs for our simulation. With about 200 localized FRBs, we can resolve the Hubble tension at 4σ while more number of localized FRBs at higher redshifts will increase the detection significance.

note that the stellar mass of our galaxy is $\approx 5 \times 10^{10} M_{\odot}$ [44] while a typical FRB host galaxy has a stellar mass of the order of $10^{10} M_{\odot}$ (Fig. 2 of [45]). Since, the DM distribution is a function of stellar mass of the host galaxy, we correct for this mismatch. To this end, we approximate the results from [10] which used the FIRE simulation [46] to obtain the host DM distribution as a function of stellar mass at high redshifts ($z \gtrsim 5$) (see Fig. 6 of [10]). The authors show the DM distribution for a few different stellar mass in the range of $10^4 - 10^{10} M_{\odot}$. The main effect of changing the galaxy stellar mass in these simulations is to shift the peak of the DM_{host} distribution, such that approximately $DM_{\text{host}} \propto M_*^{0.3}$. We use this to scale up the host DM by a factor of 2 from typical FRB host galaxy mass $10^{10} M_{\odot}$ to our galaxy with a stellar mass $5 \times 10^{10} M_{\odot}$. This is a conservative choice, without this rescaling, our conclusions described below, will only be strengthened (compared dotted black with colored solid lines). A similar dependence of the host DM on stellar mass is seen in Fig. 5 of [27] which uses IllustrisTNG (though the results can depend upon the details of the simulation).

We plot the cumulative distribution function (CDF) of the observed DM of these pulsars for a couple of cases with prescribed ages in Fig. 4. As suggested above, we note that for younger ages, the typical DM_{host} is larger. We compare these cases with our inferred results for μ_0 . We draw

samples of 100 FRBs from a lognormal distribution with mean $\mu_0 = 4$ and $\sigma_{\text{host}} = 1$ and plot their CDF (after rescaling), repeating this process many times. With a single log-normal population of DM_{host} we can exclude the scenario where the FRB progenitors are on average younger than 10 Myr at a 95 percent confidence interval. The maximum difference between the two CDFs is greater than 0.3 after accounting for noise due to one realization. By doing a Kolmogorov-Smirnov test for the 100 FRBs in our sample, the difference has to be less than 0.13 for the two CDFs to be consistent. Therefore, our results point towards progenitors with age $\gtrsim 10$ Myr. This conclusion matches with the scenario where the progenitors are typically 10-100 Myr old (Fig. 4). These results concerning a mix of star-formation following and an older population are consistent with estimates based on population modeling of FRBs without known redshift [47]. We also show the DM distribution of Galactic magnetars in the pulsar catalog. We find 6 objects with a surface magnetic field (inferred from P, \dot{P} assuming dipole radiation) of $\gtrsim 10^{14}$ G, five of which are known magnetars ³ and the sixth is the long period transient and magnetar candidate, PSR J0901–4046 [48, 49]. We also add the magnetar SGR 1935+2154 (the source of the Galactic FRB 20200428, [50, 51]) which has a reported DM of $\approx 332 \text{ pc cm}^{-3}$ [52]. The Galactic magnetar DMs are even larger than those of the youngest pulsars (this is not surprising as active magnetar ages are typically $\sim 10^4$ yrs [53]) and therefore even more discrepant with the inferred host DMs of localized FRBs.

As a crucial check of our results, we assume a bimodal distribution of host galaxy DM (μ_0) with an addition of high DM component which is contributed by magnetars. This is motivated by the fact that the sample of well studied FRBs clearly includes both sources in highly active star forming regions, with a significant DM component associated with the sources’ immediate environment and host galaxies (e.g. FRB 20121102A and FRB 20190520B, [36, 54]) and other sources, such as FRB 20200120E, which has been localized to an old environment - a globular cluster in M81, and for which the DM contribution from the source and host is constrained to be $\lesssim 20 \text{ pc cm}^{-3}$ [55, 56]. We assume this large DM component to have $\mu_{0,\text{high}} \approx 5.86$ (or $e^{\mu_{0,\text{high}}} \approx 350 \text{ pc cm}^{-3}$) and $\sigma_{\text{host}} = 1$, consistent with the population of Galactic magnetars. We assume the large DM population to be a fraction f of total population of FRBs. We fit our sample of 110 FRBs with this bimodal distribution of μ_0 (fitting $\mu_{0,\text{low}}$) in addition to varying h and f . We find that f is consistent with zero with 1σ upper limit to be 0.3. The current data is not powerful enough to constrain f at high significance, and the large DM population may still be the overall majority. Therefore, we do not pursue this issue further in this work. We note that, in this case, the estimate for h becomes $0.66^{+0.28}_{-0.16}$.

8 Scattering timescale

We consider the correlation of the scattering timescale (τ) of FRBs as a function of redshift and total DM. We tabulate a sample of localized FRBs in Table 1 with associated τ or available upper limits. We have taken the observed frequency to be at 1 GHz and have converted available data at different frequencies assuming $\tau \propto \nu^{-4.4}$. We also show the stellar mass and the star formation rate (SFR) of the host galaxy along with galaxy type. In upper left panel of Fig. 5, we plot the observed

³<https://www.physics.mcgill.ca/pulsar/magnetar/main.html>

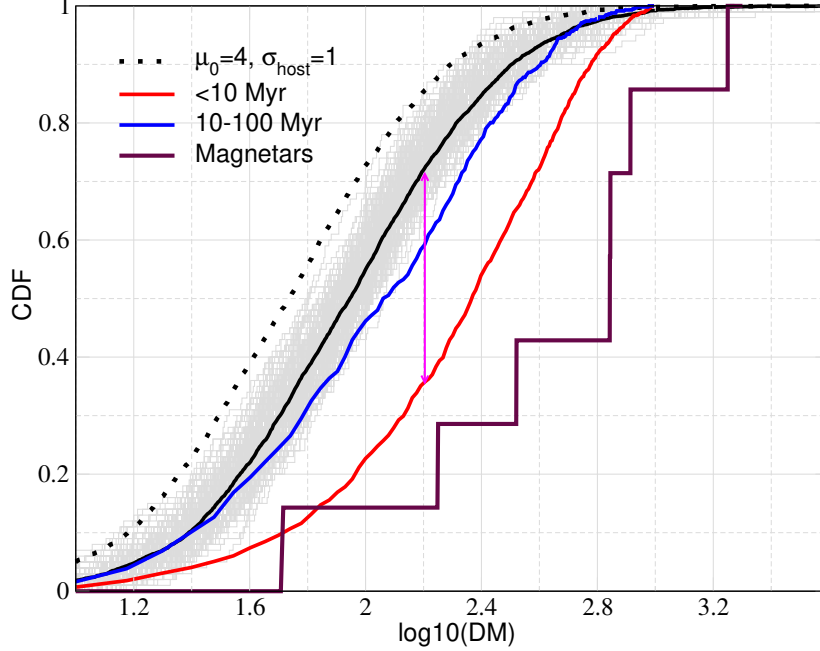


Figure 4: Comparison of cumulative distribution function (CDF) of our inferred host DM contribution with measurements of pulsars in our galaxy as a function of age. In dashed and solid black, we consider our inferred best fit value of $\mu_0 = 4$ and the rescaled version respectively. We consider a sample of 5000 FRBs to obtain a smooth curve. We also plot realizations where we sample 100 FRBs from a lognormal distribution with $\mu_0 = 4$ and $\sigma_{\text{host}} = 1$, in grey. We plot the CDF of galactic pulsars in solid red. In the double-headed magenta line, we show the maximum difference between the black solid and red solid lines which is used for the Kolmogorov-Smirnov test (see §7). We also show the CDF of galactic magnetars.

τ vs the observed DM. The data is suggestive of a potential correlation between observed τ and DM_{obs} . Previously, The authors in [57] and [58] have noted the correlation between τ and extragalactic component of DM for unlocalized FRBs. As the measured scattering is generally inconsistent with expectations from the IGM [59], this could suggest an underlying correlation between τ and DM_{host} . We also plot the measurements from the CHIME catalog [60] which do not show any significant correlation between τ and DM_{obs} . For the sample of localized FRBs studied here, we compute the expected τ from our galaxy using the fit obtained in [61]. We show them in vertical lines with error bars in Fig. 5 (top right panel). Only 4 of these FRBs are consistent with Galactic τ . We exclude these 4 FRBs from further analysis. We define τ_{rf} as the scattering timescale in the host galaxy rest frame (at 1 GHz). Assuming $\tau \propto \nu^{-4.4}$ (as typically expected for a Kolmogorov spectrum of turbulence, see [59]), τ_{rf} is related to the observed τ by the relation, $\tau_{\text{rf}} = \tau(1+z)^{3.4}$ where z is the redshift of the host galaxy. We plot τ_{rf} as a function of z (upper right panel). We do not find a strong correlation between $\log\tau_{\text{rf}}$ and z (Pearson correlation coefficient $r = 0.27$ and $p\text{-value} = 0.35$), suggesting that any $\tau\text{-DM}_{\text{obs}}$ correlation is more likely driven the host galaxy (+ source) contribution.

In the bottom left panel of Fig. 5, we plot our estimate of host galaxy DM as a function of τ_{rf} . Our estimate follows from Eq. 2.1 with $\text{DM}_{\text{host,est}} = (\text{DM}_{\text{obs}} - \text{DM}_{\text{halo}} - \text{DM}_{\text{ISM}} - \langle \text{DM}_{\text{IGM}} \rangle)(1 + z)$ where $\langle \text{DM}_{\text{IGM}} \rangle$ follows from Eq. 3.1. For some of the objects our estimated host DM is negative which is expected since the IGM component varies along line of sight in contrast to our assumption in the equation above. We see a hint of correlation between τ_{rf} and $\text{DM}_{\text{host,est}}$ (r coefficient=0.745, p -value=0.002). We also plot τ_{rf} as a function of stellar mass and SFR. Most of the host galaxies are starforming and they show a significant scatter in their star formation rate, stellar mass, and their ratio (the specific star formation rate). There are two transitioning galaxies and one quiescent galaxy in this sample. Overall, with this small sample, there is no significant correlation between τ_{rf} and these galaxy properties and no clear difference between the transitioning and starforming galaxies. This may suggest that scatter broadening is dominated by the immediate surrounding environment rather than the host galaxy. However, we need a bigger sample with more quiescent galaxies to test whether the scattering timescale can be a good proxy to test FRB host galaxy environment.

FRB	z	$\log_{10}(M_*) M_{\odot}$	$\text{SFR} (M_{\odot} \text{ yr}^{-1})$	τ (ms)	galaxy type	References
20181030A	0.0039	9.76	0.35	< 0.18	starforming	[60]
20181220A	0.027	$9.86^{0.14}_{-0.12}$	$2.9^{1.6}_{-0.9}$	0.059 ± 0.004	starforming	[60]
20181223C	0.03	$9.29^{0.16}_{-0.20}$	$0.15^{0.12}_{-0.08}$	0.013 ± 0.003	starforming	[60]
20190425A	0.031	$10.26^{0.09}_{-0.1}$	$1.6^{1.5}_{-0.9}$	< 0.049	starforming	[60]
20180916	0.0337	$9.91^{0.03}_{-0.05}$	$0.04^{0.03}_{-0.02}$	0.022	starforming	[62]
20201123	0.0507	11.2	0.2	7.5	starforming	[63]
20210405I	0.066	11.25	0.3	9.7 ± 0.2	starforming	[64]
20190418A	0.071	$10.27^{0.13}_{-0.17}$	$0.8^{1.1}_{-0.6}$	< 0.1	starforming	[60]
20220509	0.0894	10.7 ± 0.01	$0.25^{0.07}_{-0.04}$	0.3 ± 0.07	starforming	[65]
20190608	0.1178	10.56 ± 0.02	$7.03^{1.43}_{-1.15}$	8.65 ± 0.52	starforming	[66]
20190110C	0.1224	10.748	0.59	0.028 ± 0.004	transitioning	[60]
20240209	0.1384	11.35 ± 0.01	< 0.31	< 0.026	quiescent	[67, 68]
20210410	0.1415	9.47 ± 0.05	$0.03^{0.03}_{-0.01}$	29.4 ± 2.8	transitioning	[69]
20210603A	0.177	10.93 ± 0.04	0.24 ± 0.06	0.02 ± 0.0004	starforming	[70]
20121102A	0.193	$8.14^{0.09}_{-0.10}$	$0.05^{0.02}_{-0.01}$	$\lesssim 0.6$	starforming	[71]
20210117A	0.214	$8.56^{0.06}_{-0.08}$	$0.014^{0.008}_{-0.004}$	0.86	starforming	[72]
20191001	0.234	$10.73^{0.07}_{-0.08}$	$18.28^{17.24}_{-8.95}$	1.52 ± 0.92	starforming	[73]
20190714	0.2365	10.22 ± 0.04	$1.89^{1.22}_{-0.72}$	$\lesssim 2.23$	starforming	[74]
20190520B	0.241	$9.08^{0.08}_{-0.09}$	$0.04^{0.04}_{-0.02}$	41.99 ± 5.75	starforming	[75]
20190102	0.2913	$9.69^{0.09}_{-0.11}$	$0.4^{0.31}_{-0.11}$	0.1 ± 0.005	starforming	[66]
20180924	0.3212	10.3 ± 0.02	$0.62^{0.32}_{-0.24}$	1.2 ± 0.04	starforming	[76]

FRB	z	$\log_{10}(M_*) M_\odot$	SFR ($M_\odot \text{ yr}^{-1}$)	τ (ms)	galaxy type	References
20190611	0.3778	9.57 ± 0.12	$0.53^{0.77}_{-0.26}$	0.47 ± 0.52	starforming	[66]
20190711	0.5220	$9.1^{0.15}_{-0.23}$	$0.95^{0.96}_{-0.5}$	$\lesssim 3.2$	starforming	[74]
20220610A	1.016	9.7	1.7	0.89	starforming	[77]

Table 1: List of localized FRBs with measured scattering timescales at 1 GHz, their stellar mass, star formation rate which are used to obtain results in this section. We also provide the error bars in these measurements wherever available.

9 Conclusions

We have tested some cosmological and astrophysical implications of the observed sample of FRBs with known z . First, we infer the Hubble constant using a sample of 110 localized FRBs. This requires inputs from cosmological simulations. We have used results from two simulations and show that they give consistent results at present. Our inferred H_0 is consistent with both low and high redshift measurements at 1σ confidence interval. We project that with ~ 200 localized FRBs, we should be able to distinguish between the two measurements at 4σ confidence interval. This projection depends upon the redshift distribution of the sample of FRBs with known z . At high redshifts, the cosmological component of the DM dominates over the host DM contribution. Therefore, the observed DM is polluted less by the host DM and we have a better chance to distill H_0 from the dominant cosmological component. Projecting towards the future, FRBs can provide a unique angle on the Hubble tension debate. The reason is that the measurement of H_0 with FRBs can in principle be done over a wide range of redshifts, up to the era of H reionization [10]. This can allow to get a low and high z estimate of H_0 using a single technique and to determine whether the Hubble tension is due to measurement systematics or whether it is indicative of new physics.

We have emphasized in this work the importance of simultaneously inferring H_0 and μ_0 (the host DM contribution) in order to make the best and most reliable use of FRB data to infer cosmological parameters. The inferred DM_{host} is typically $\sim 60 \text{ pc cm}^{-3}$, much smaller than young pulsars and magnetars in the Milky Way, for which the measured values are on average at least four times larger. While a small part of this difference (factor of $\lesssim 2$) is potentially driven by the difference in stellar mass between typical FRB hosts and the Milky Way, a significant deviation still remains. Taken at face value this can be used to exclude young FRB progenitors with age $\lesssim 10 \text{ Myr}$ at a 95 percent confidence interval. That being said, our methodology, as applied to the current data, can only obtain broad characteristics of the FRB DM_{host} population and cannot exclude even a tens of percent sub-population with much larger DM_{host} , consistent with young magnetars / pulsars. An indication of a potentially bimodal of FRB source ages (and DM_{host}) is motivated by the contrast between the environments of FRBs such as 20121102A and 20190520B and that of, e.g. FRB 20200120E. In addition, studying the observed population of non-localized FRBs [47] have recently shown that such a bimodal population of FRB source ages describes the current data better than a single (star formation following or mass

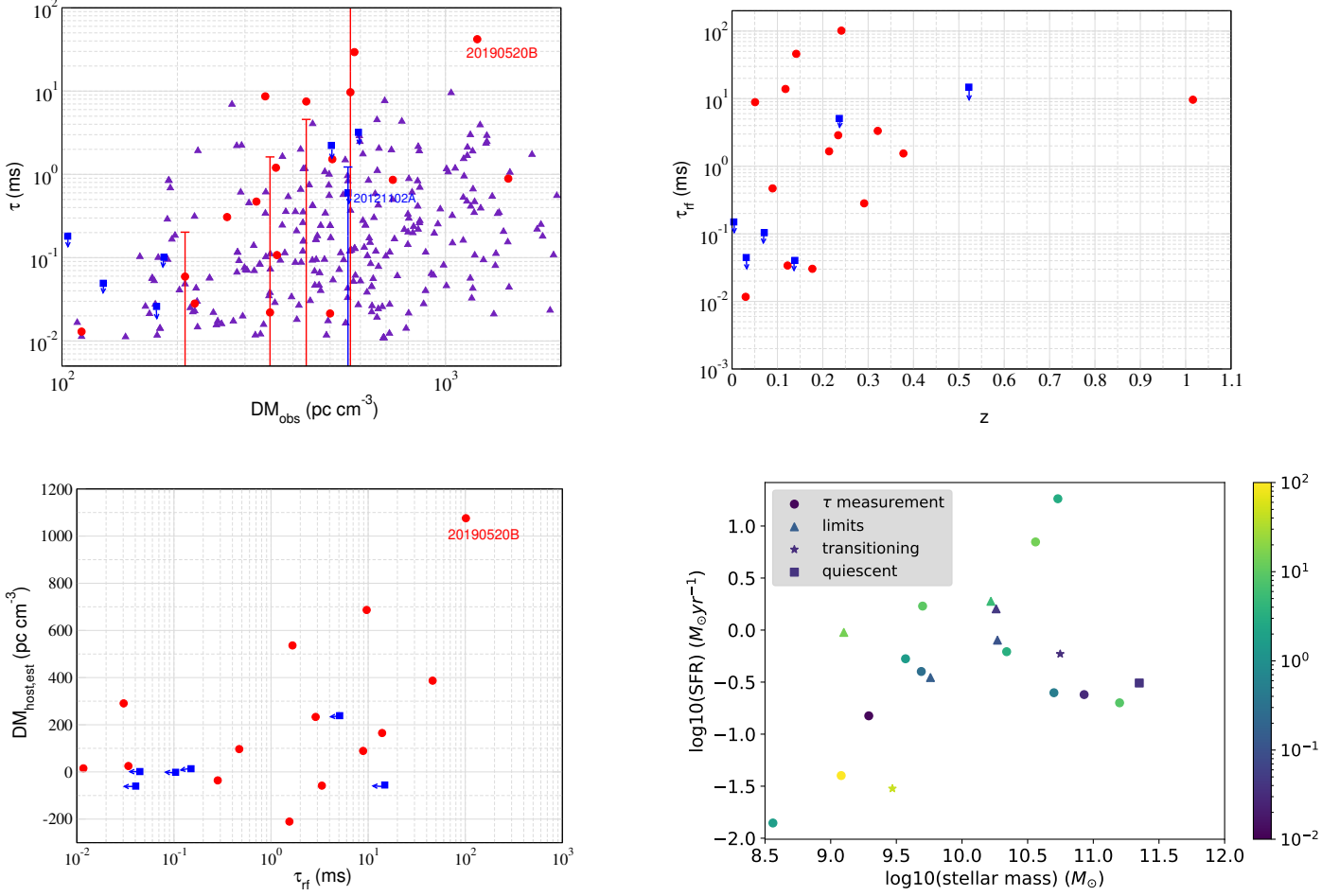


Figure 5: Dependence of τ as a function of other FRB properties. Upper left: observed τ vs observed DM. The corresponding Milky Way contribution to τ is shown with errorbars using the model of [61] and is consistent with measured values in 4 FRBs (these are excluded in the following). We also show the CHIME catalogue in triangle points [60]. Upper right: τ_{ff} (rest frame of host galaxy) vs z . Lower left: Our rough estimate of host galaxy DM (see text) as a function of τ_{ff} . Lower right: τ_{ff} as a function of stellar mass and star formation rate (circles and triangles denote cases with measured τ and its upper limit correspondingly). The two transitioning galaxies are denoted by stars. The quiescent galaxy which has a lower limit on τ is denoted by a square.

following) population. Furthermore, as reported in the first CHIME catalogue, CHIME detected bursts have an observational selection effect against detecting highly scattered FRBs, with $\tau \gtrsim 100$ ms [78]. As long scatter broadening times are potentially correlated with larger DM_{host} (see figure 5), the intrinsic population of large DM_{host} FRBs might even be larger than the low DM_{host} population.

Finally, we have considered the correlation between the observed scattering timescale and observed DM. Our sample of FRBs with scattering timescale measurements is dominated by starforming

galaxies, with just two transitioning galaxy hosts and one quiescent galaxy. The starforming galaxies show significant variation in their associated specific star formation rate and these broad galaxy characteristics aren't strongly correlated with the scattering timescale. There is a tentative correlation between the scatter broadening time and the DM_{host} estimates, suggesting that scattering may be dominated by the more immediate environments of FRB sources rather than the host galaxy interstellar medium. For a turbulent plasma screen, one expects $\tau_{\text{rf}} \propto \nu^{-22/5} d_{\text{scr}} DM_{\text{scr}}^{12/5}$ (e.g. [79]), where d_{scr} is the distance of the screen from the source and DM_{scr} is the dispersion measure associated with the screen. A correlation between τ_{rf} and DM_{host} is therefore expected to be most clearly visible in bursts with large $\tau_{\text{rf}} / \text{excess DM}$, for which the plasma screen would dominate both. Indeed, in a recent work, [80] have shown that the immediate environment of FRB 20190520B, has a sSFR that is ≥ 3 times larger the average value within the host. Considering that this source is also the largest in our sample in terms of its $\tau_{\text{rf}} / \text{excess DM}$, this is highly suggestive of those properties being dominated by the near environment of the source, rather than the ISM of its host galaxy. A larger sample of localized FRBs with constraints on scatter broadening and galaxy properties and more in-depth observations of their environments (e.g. constraining $H\alpha$ emission) will be needed to test this picture.

Acknowledgements

We thank Pawan Kumar and Om Gupta for helpful discussions. SKA is supported by the ARCO fellowship. PB is supported by a grant (no. 2020747) from the United States-Israel Binational Science Foundation (BSF), Jerusalem, Israel, by a grant (no. 1649/23) from the Israel Science Foundation and by a grant (no. 80NSSC 24K0770) from the NASA astrophysics theory program.

References

- [1] Liam Connor, Vikram Ravi, Kritti Sharma, Stella Koch Ocker, Jakob Faber, Gregg Hallinan, Charlie Harnach, Greg Hellbourg, Rick Hobbs, David Hodge, Mark Hodges, Nikita Kosogorov, James Lamb, Casey Law, Paul Rasmussen, Myles Sherman, Jean Somalwar, Sander Weinreb, and David Woody. A gas rich cosmic web revealed by partitioning the missing baryons. [arXiv e-prints](#), page arXiv:2409.16952, September 2024. [arXiv:2409.16952](#), [DOI], [ADS].
- [2] D. H. Gao, Q. Wu, J. P. Hu, S. X. Yi, X. Zhou, and F. Y. Wang. Measuring Hubble constant using localized and unlocalized fast radio bursts. [arXiv e-prints](#), page arXiv:2410.03994, October 2024. [arXiv:2410.03994](#), [DOI], [ADS].
- [3] Eduard Fernando Piratova-Moreno, Luz Ángela García, Carlos A. Benavides-Gallego, and Carolina Cabrera. Fast Radio Bursts as cosmological proxies: estimating the Hubble constant. [arXiv e-prints](#), page arXiv:2502.08509, February 2025. [arXiv:2502.08509](#), [DOI], [ADS].
- [4] Matthew McQuinn. Locating the “Missing” Baryons with Extragalactic Dispersion Measure Estimates. [ApJL](#), 780(2):L33, January 2014. [arXiv:1309.4451](#), [DOI], [ADS].
- [5] David Eichler. Nanolensed Fast Radio Bursts. [ApJ](#), 850(2):159, December 2017. [arXiv:1711.04764](#), [DOI], [ADS].
- [6] Adi Zitrin and David Eichler. Observing Cosmological Processes in Real Time with Repeating Fast Radio Bursts. [ApJ](#), 866(2):101, October 2018. [arXiv:1807.03287](#), [DOI], [ADS].

- [7] Zheng-Xiang Li, He Gao, Xu-Heng Ding, Guo-Jian Wang, and Bing Zhang. Strongly lensed repeating fast radio bursts as precision probes of the universe. *Nature Communications*, 9:3833, September 2018. [arXiv:1708.06357](#), [DOI], [ADS].
- [8] Pawan Kumar and Eric V. Linder. Use of fast radio burst dispersion measures as distance measures. *Phys.Rev.D*, 100(8):083533, October 2019. [arXiv:1903.08175](#), [DOI], [ADS].
- [9] J. P. Macquart, J. X. Prochaska, M. McQuinn, K. W. Bannister, S. Bhandari, C. K. Day, A. T. Deller, R. D. Ekers, C. W. James, L. Marnoch, S. Osłowski, C. Phillips, S. D. Ryder, D. R. Scott, R. M. Shannon, and N. Tejos. A census of baryons in the Universe from localized fast radio bursts. *Nature*, 581(7809):391–395, May 2020. [arXiv:2005.13161](#), [DOI], [ADS].
- [10] Paz Beniamini, Pawan Kumar, Xiangcheng Ma, and Eliot Quataert. Exploring the epoch of hydrogen reionization using FRBs. *MNRAS*, 502(4):5134–5146, April 2021. [arXiv:2011.11643](#), [DOI], [ADS].
- [11] Steffen Hagstotz, Robert Reischke, and Robert Lilow. A new measurement of the Hubble constant using fast radio bursts. *MNRAS*, 511(1):662–667, March 2022. [arXiv:2104.04538](#), [DOI], [ADS].
- [12] C. W. James, E. M. Ghosh, J. X. Prochaska, K. W. Bannister, S. Bhandari, C. K. Day, A. T. Deller, M. Glowacki, A. C. Gordon, K. E. Heintz, L. Marnoch, S. D. Ryder, D. R. Scott, R. M. Shannon, and N. Tejos. A measurement of Hubble’s Constant using Fast Radio Bursts. *MNRAS*, 516(4):4862–4881, November 2022. [arXiv:2208.00819](#), [DOI], [ADS].
- [13] Qin Wu, Guo-Qiang Zhang, and Fa-Yin Wang. An 8 per cent determination of the Hubble constant from localized fast radio bursts. *MNRAS*, 515(1):L1–L5, September 2022. [arXiv:2108.00581](#), [DOI], [ADS].
- [14] Bing Zhang. The physics of fast radio bursts. *Reviews of Modern Physics*, 95(3):035005, July 2023. [arXiv:2212.03972](#), [DOI], [ADS].
- [15] Ilya S. Khrykin, Metin Ata, Khee-Gan Lee, Sunil Simha, Yuxin Huang, J. Xavier Prochaska, Nicolas Tejos, Keith W. Bannister, Jeff Cooke, Cherie K. Day, Adam Deller, Marcin Glowacki, Alexa C. Gordon, Clancy W. James, Lachlan Marnoch, Ryan. M. Shannon, Jielai Zhang, and Lucas Bernales-Cortes. FLIMFLAM DR1: The First Constraints on the Cosmic Baryon Distribution from 8 FRB sightlines. *arXiv e-prints*, page arXiv:2402.00505, February 2024. [arXiv:2402.00505](#), [DOI], [ADS].
- [16] Abinash Kumar Shaw, Raghunath Ghara, Paz Beniamini, Saleem Zaroubi, and Pawan Kumar. Asking Fast Radio Bursts (FRBs) for More than Reionization History. *arXiv e-prints*, page arXiv:2409.03255, September 2024. [arXiv:2409.03255](#), [DOI], [ADS].
- [17] Planck Collaboration. Planck 2018 results. VI. Cosmological parameters. *A&A*, 641:A6, September 2020. [arXiv:1807.06209](#), [DOI], [ADS].
- [18] Adam G. Riess, Stefano Casertano, Wenlong Yuan, Lucas M. Macri, and Dan Scolnic. Large Magellanic Cloud Cepheid Standards Provide a 1% Foundation for the Determination of the Hubble Constant and Stronger Evidence for Physics beyond Λ CDM. *ApJ*, 876(1):85, May 2019. [arXiv:1903.07603](#), [DOI], [ADS].
- [19] Licia Verde, Tommaso Treu, and Adam G. Riess. Tensions between the early and late Universe. *Nature Astronomy*, 3:891–895, September 2019. [arXiv:1907.10625](#), [DOI], [ADS].
- [20] Anthony Walters, Amanda Weltman, B. M. Gaensler, Yin-Zhe Ma, and Amadeus Witzemann. Future

- Cosmological Constraints From Fast Radio Bursts. *ApJ*, 856(1):65, March 2018. [arXiv:1711.11277](#), [\[DOI\]](#), [\[ADS\]](#).
- [21] Ze-Wei Zhao, Zheng-Xiang Li, Jing-Zhao Qi, He Gao, Jing-Fei Zhang, and Xin Zhang. Cosmological Parameter Estimation for Dynamical Dark Energy Models with Future Fast Radio Burst Observations. *ApJ*, 903(2):83, November 2020. [arXiv:2006.01450](#), [\[DOI\]](#), [\[ADS\]](#).
- [22] Steffen Hagstotz, Robert Reischke, and Robert Lilow. A new measurement of the Hubble constant using fast radio bursts. *MNRAS*, 511(1):662–667, March 2022. [arXiv:2104.04538](#), [\[DOI\]](#), [\[ADS\]](#).
- [23] Qin Wu, Guo-Qiang Zhang, and Fa-Yin Wang. An 8 per cent determination of the Hubble constant from localized fast radio bursts. *MNRAS*, 515(1):L1–L5, September 2022. [arXiv:2108.00581](#), [\[DOI\]](#), [\[ADS\]](#).
- [24] Yang Liu, Hongwei Yu, and Puxun Wu. Cosmological-model-independent Determination of Hubble Constant from Fast Radio Bursts and Hubble Parameter Measurements. *ApJL*, 946(2):L49, April 2023. [arXiv:2210.05202](#), [\[DOI\]](#), [\[ADS\]](#).
- [25] Jéferson A. S. Fortunato, Wiliam S. Hipólito-Ricaldi, and Marcelo V. dos Santos. Cosmography from well-localized fast radio bursts. *MNRAS*, 526(2):1773–1782, December 2023. [arXiv:2307.04711](#), [\[DOI\]](#), [\[ADS\]](#).
- [26] Sandeep Kumar Acharya and Paz Beniamini. Redshift dependence of FRB host dispersion measures across cosmic epochs. *JCAP*, 2025(1):036, January 2025. [arXiv:2408.03163](#), [\[DOI\]](#), [\[ADS\]](#).
- [27] Jian-Feng Mo, Weishan Zhu, Yang Wang, Lin Tang, and Long-Long Feng. The dispersion measure of Fast Radio Bursts host galaxies: estimation from cosmological simulations. *MNRAS*, 518(1):539–561, January 2023. [arXiv:2210.14052](#), [\[DOI\]](#), [\[ADS\]](#).
- [28] Annalisa Pillepich, Volker Springel, Dylan Nelson, Shy Genel, Jill Naiman, Rüdiger Pakmor, Lars Hernquist, Paul Torrey, Mark Vogelsberger, Rainer Weinberger, and Federico Marinacci. Simulating galaxy formation with the IllustrisTNG model. *MNRAS*, 473(3):4077–4106, January 2018. [arXiv:1703.02970](#), [\[DOI\]](#), [\[ADS\]](#).
- [29] Pierre Ocvirk, Dominique Aubert, Jenny G. Sorce, Paul R. Shapiro, Nicolas Deparis, Taha Dawoodbhoy, Joseph Lewis, Romain Teyssier, Gustavo Yepes, Stefan Gottlöber, Kyungjin Ahn, Ilian T. Iliev, and Yehuda Hoffman. Cosmic Dawn II (CoDa II): a new radiation-hydrodynamics simulation of the self-consistent coupling of galaxy formation and reionization. *MNRAS*, 496(4):4087–4107, August 2020. [arXiv:1811.11192](#), [\[DOI\]](#), [\[ADS\]](#).
- [30] Sanskriti Das, Smita Mathur, Anjali Gupta, Fabrizio Nicastro, and Yair Krongold. Empirical estimates of the Galactic halo contribution to the dispersion measures of extragalactic fast radio bursts using X-ray absorption. *MNRAS*, 500(1):655–662, January 2021. [arXiv:2007.11542](#), [\[DOI\]](#), [\[ADS\]](#).
- [31] J. M. Cordes and T. J. W. Lazio. NE2001.I. A New Model for the Galactic Distribution of Free Electrons and its Fluctuations. *arXiv e-prints*, page 0207156, July 2002. [arXiv:0207156](#), [\[DOI\]](#), [\[ADS\]](#).
- [32] J. M. Yao, R. N. Manchester, and N. Wang. A New Electron-density Model for Estimation of Pulsar and FRB Distances. *ApJ*, 835(1):29, January 2017. [arXiv:1610.09448](#), [\[DOI\]](#), [\[ADS\]](#).
- [33] G. H. Hilmarsson, D. Michilli, L. G. Spitler, R. S. Wharton, P. Demorest, G. Desvignes, K. Gourdji, S. Hackstein, J. W. T. Hessels, K. Nimmo, A. D. Seymour, M. Kramer, and R. Mckinven. Rotation Measure Evolution of the Repeating Fast Radio Burst Source FRB 121102. *ApJL*, 908(1):L10, February 2021. [arXiv:2009.12135](#), [\[DOI\]](#), [\[ADS\]](#).

- [34] Reshma Anna-Thomas et al. Magnetic field reversal in the turbulent environment around a repeating fast radio burst. *Science*, 380(6645):599–603, May 2023. [arXiv:2202.11112](#), [DOI], [ADS].
- [35] S. Chatterjee, C. J. Law, R. S. Wharton, S. Burke-Spolaor, J. W. T. Hessels, G. C. Bower, J. M. Cordes, S. P. Tendulkar, C. G. Bassa, P. Demorest, B. J. Butler, A. Seymour, P. Scholz, M. W. Abruzzo, S. Bogdanov, V. M. Kaspi, A. Keimpema, T. J. W. Lazio, B. Marcote, M. A. McLaughlin, Z. Paragi, S. M. Ransom, M. Rupen, L. G. Spitler, and H. J. van Langevelde. A direct localization of a fast radio burst and its host. *Nature*, 541(7635):58–61, January 2017. [arXiv:1701.01098](#), [DOI], [ADS].
- [36] C. H. Niu, K. Aggarwal, D. Li, X. Zhang, S. Chatterjee, C. W. Tsai, W. Yu, C. J. Law, S. Burke-Spolaor, J. M. Cordes, Y. K. Zhang, S. K. Ocker, J. M. Yao, P. Wang, Y. Feng, Y. Niino, C. Bochenek, M. Cruces, L. Connor, J. A. Jiang, S. Dai, R. Luo, G. D. Li, C. C. Miao, J. R. Niu, R. Anna-Thomas, J. Sydnor, D. Stern, W. Y. Wang, M. Yuan, Y. L. Yue, D. J. Zhou, Z. Yan, W. W. Zhu, and B. Zhang. A repeating fast radio burst associated with a persistent radio source. *Nature*, 606(7916):873–877, June 2022. [arXiv:2110.07418](#), [DOI], [ADS].
- [37] Joshua J. Ziegler, Paul R. Shapiro, Taha Dawoodbhoj, Paz Beniamini, Pawan Kumar, Katherine Freese, Pierre Ocvirk, Dominique Aubert, Joseph S. W. Lewis, Romain Teyssier, Hyunbae Park, Kyungjin Ahn, Jenny G. Sorce, Ilian T. Iliev, Gustavo Yepes, and Stefan Gottlober. Dispersion Measures of Fast Radio Bursts through the Epoch of Reionization. *arXiv e-prints*, page arXiv:2411.02699, November 2024. [arXiv:2411.02699](#), [DOI], [ADS].
- [38] Z. J. Zhang, K. Yan, C. M. Li, G. Q. Zhang, and F. Y. Wang. Intergalactic Medium Dispersion Measures of Fast Radio Bursts Estimated from IllustrisTNG Simulation and Their Cosmological Applications. *ApJ*, 906(1):49, January 2021. [arXiv:2011.14494](#), [DOI], [ADS].
- [39] G. Q. Zhang, Hai Yu, J. H. He, and F. Y. Wang. Dispersion Measures of Fast Radio Burst Host Galaxies Derived from IllustrisTNG Simulation. *ApJ*, 900(2):170, September 2020. [arXiv:2007.13935](#), [DOI], [ADS].
- [40] Dylan Nelson, Volker Springel, Annalisa Pillepich, Vicente Rodriguez-Gomez, Paul Torrey, Shy Genel, Mark Vogelsberger, Ruediger Pakmor, Federico Marinacci, Rainer Weinberger, Luke Kelley, Mark Lovell, Benedikt Diemer, and Lars Hernquist. The IllustrisTNG simulations: public data release. *Computational Astrophysics and Cosmology*, 6(1):2, May 2019. [arXiv:1812.05609](#), [DOI], [ADS].
- [41] J. P. Macquart and RD Ekers. FRB event rate counts - II. Fluence, redshift, and dispersion measure distributions. *MNRAS*, 480(3):4211–4230, November 2018. [arXiv:1808.00908](#), [DOI], [ADS].
- [42] Gregg Hallinan, Vikram Ravi, Katie Bouman, Fabian Walter, Francois Kapp, Katie Jameson, and DSA-2000 collaboration. The DSA-2000 Radio Camera. In *American Astronomical Society Meeting Abstracts*, volume 243 of *American Astronomical Society Meeting Abstracts*, page 237.05, February 2024. [ADS].
- [43] Keith Vanderlinde, Adrian Liu, Bryan Gaensler, Dick Bond, Gary Hinshaw, Cherry Ng, Cynthia Chiang, Ingrid Stairs, Jo-Anne Brown, Jonathan Sievers, Juan Mena, Kendrick Smith, Kevin Bandura, Kiyoshi Masui, Kristine Spekkens, Leo Belostotski, Matt Dobbs, Neil Turok, Patrick Boyle, Michael Rupen, Tom Landecker, Ue-Li Pen, and Victoria Kaspi. The Canadian Hydrogen Observatory and Radio-transient Detector (CHORD). In *Canadian Long Range Plan for Astronomy and Astrophysics White Papers*, volume 2020, page 28, October 2019. [arXiv:1911.01777](#), [DOI], [ADS].
- [44] F. Hammer, M. Puech, L. Chemin, H. Flores, and M. D. Lehnert. The Milky Way, an Exceptionally

- Quiet Galaxy: Implications for the Formation of Spiral Galaxies. *ApJ*, 662(1):322–334, June 2007. [arXiv:astro-ph/0702585](#), [DOI], [ADS].
- [45] Kritti Sharma et al. Preferential Occurrence of Fast Radio Bursts in Massive Star-Forming Galaxies. *arXiv e-prints*, page arXiv:2409.16964, September 2024. [arXiv:2409.16964](#), [DOI], [ADS].
- [46] Xiangcheng Ma, Philip F. Hopkins, Shea Garrison-Kimmel, Claude-André Faucher-Giguère, Eliot Quataert, Michael Boylan-Kolchin, Christopher C. Hayward, Robert Feldmann, and Dušan Kereš. Simulating galaxies in the reionization era with FIRE-2: galaxy scaling relations, stellar mass functions, and luminosity functions. *MNRAS*, 478(2):1694–1715, August 2018. [arXiv:1706.06605](#), [DOI], [ADS].
- [47] Om Gupta, Paz Beniamini, Pawan Kumar, and Steven L. Finkelstein. The cosmic evolution of FRBs inferred from CHIME/FRB Catalog 1. *arXiv e-prints*, page arXiv:2501.09810, January 2025. [arXiv:2501.09810](#), [DOI], [ADS].
- [48] Manisha Caleb, Ian Heywood, Kaustubh Rajwade, Mateusz Malenta, Benjamin Willem Stappers, Ewan Barr, Weiwei Chen, Vincent Morello, Sotiris Sanidas, Jakob van den Eijnden, Michael Kramer, David Buckley, Jaco Brink, Sara Elisa Motta, Patrick Woudt, Patrick Weltevrede, Fabian Jankowski, Mayuresh Surnis, Sarah Buchner, Mechiel Christiaan Bezuidenhout, Laura Nicole Driessen, and Rob Fender. Discovery of a radio-emitting neutron star with an ultra-long spin period of 76 s. *Nature Astronomy*, 6:828–836, May 2022. [arXiv:2206.01346](#), [DOI], [ADS].
- [49] P. Beniamini, Z. Wadiasingh, J. Hare, K. M. Rajwade, G. Younes, and A. J. van der Horst. Evidence for an abundant old population of Galactic ultra-long period magnetars and implications for fast radio bursts. *MNRAS*, 520(2):1872–1894, April 2023. [arXiv:2210.09323](#), [DOI], [ADS].
- [50] B. C. CHIME/FRB Collaboration, Andersen, K. M. Bandura, M. Bhardwaj, A. Bij, M. M. Boyce, P. J. Boyle, C. Brar, T. Cassanelli, P. Chawla, T. Chen, J. F. Cliche, A. Cook, D. Cubranic, A. P. Curtin, N. T. Denman, M. Dobbs, F. Q. Dong, M. Fandino, E. Fonseca, B. M. Gaensler, U. Giri, D. C. Good, M. Halpern, A. S. Hill, G. F. Hinshaw, C. Höfer, A. Josephy, J. W. Kania, V. M. Kaspi, T. L. Landecker, C. Leung, D. Z. Li, H. H. Lin, K. W. Masui, R. McKinven, J. Mena-Parra, M. Merryfield, B. W. Meyers, D. Michilli, N. Milutinovic, A. Mirhosseini, M. Münchmeyer, A. Naidu, L. B. Newburgh, C. Ng, C. Patel, U. L. Pen, T. Pinsonneault-Marotte, Z. Pleunis, B. M. Quine, M. Rafiei-Ravandi, M. Rahman, S. M. Ransom, A. Renard, P. Sanghavi, P. Scholz, J. R. Shaw, K. Shin, S. R. Siegel, S. Singh, R. J. Smegal, K. M. Smith, I. H. Stairs, C. M. Tan, S. P. Tendulkar, I. Tretyakov, K. Vanderlinde, H. Wang, D. Wulf, and A. V. Zwaniga. A bright millisecond-duration radio burst from a Galactic magnetar. *Nature*, 587(7832):54–58, November 2020. [arXiv:2005.10324](#), [DOI], [ADS].
- [51] C. D. Bochenek, V. Ravi, K. V. Belov, G. Hallinan, J. Kocz, S. R. Kulkarni, and D. L. McKenna. A fast radio burst associated with a Galactic magnetar. *Nature*, 587(7832):59–62, November 2020. [arXiv:2005.10828](#), [DOI], [ADS].
- [52] Paul Scholz and Chime/Frb Collaboration. A bright millisecond-timescale radio burst from the direction of the Galactic magnetar SGR 1935+2154. *The Astronomer’s Telegram*, 13681:1, April 2020. [ADS].
- [53] Paz Beniamini, Kenta Hotokezaka, Alexander van der Horst, and Chryssa Kouveliotou. Formation rates and evolution histories of magnetars. *MNRAS*, 487(1):1426–1438, July 2019. [arXiv:1903.06718](#), [DOI], [ADS].
- [54] J. N. Jahns, L. G. Spitler, K. Nimmo, D. M. Hewitt, M. P. Snelders, A. Seymour, J. W. T. Hessels, K. Gourdji, D. Michilli, and G. H. Hilmarsson. The FRB 20121102A November rain in 2018 observed

- with the Arecibo Telescope. *MNRAS*, 519(1):666–687, February 2023. [arXiv:2202.05705](#), [\[DOI\]](#), [\[ADS\]](#).
- [55] M. Bhardwaj, A. Yu. Kirichenko, D. Michilli, Y. D. Mayya, V. M. Kaspi, B. M. Gaensler, M. Rahman, S. P. Tendulkar, E. Fonseca, Alexander Josephy, C. Leung, Marcus Merryfield, Emily Petroff, Z. Pleunis, Pranav Sanghavi, P. Scholz, K. Shin, Kendrick M. Smith, and I. H. Stairs. A Local Universe Host for the Repeating Fast Radio Burst FRB 20181030A. *ApJL*, 919(2):L24, October 2021. [arXiv:2108.12122](#), [\[DOI\]](#), [\[ADS\]](#).
- [56] F. Kirsten et al. A repeating fast radio burst source in a globular cluster. *Nature*, 602(7898):585–589, February 2022. [arXiv:2105.11445](#), [\[DOI\]](#), [\[ADS\]](#).
- [57] Vikram Ravi. The observed properties of fast radio bursts. *MNRAS*, 482(2):1966–1978, January 2019. [arXiv:1710.08026](#), [\[DOI\]](#), [\[ADS\]](#).
- [58] V. Gupta, C. Flynn, W. Farah, M. Bailes, A. T. Deller, C. K. Day, and M. E. Lower. The ultranarrow FRB20191107B, and the origins of FRB scattering. *MNRAS*, 514(4):5866–5878, August 2022. [arXiv:2209.00311](#), [\[DOI\]](#), [\[ADS\]](#).
- [59] Paz Beniamini and Pawan Kumar. What does FRB light-curve variability tell us about the emission mechanism? *MNRAS*, 498(1):651–664, August 2020. [arXiv:2007.07265](#), [\[DOI\]](#), [\[ADS\]](#).
- [60] CHIME/FRB Collaboration and Amiri et al. The First CHIME/FRB Fast Radio Burst Catalog. *ApJS*, 257(2):59, December 2021. [arXiv:2106.04352](#), [\[DOI\]](#), [\[ADS\]](#).
- [61] J. M. Cordes, R. S. Wharton, L. G. Spitler, S. Chatterjee, and I. Wasserman. Radio Wave Propagation and the Provenance of Fast Radio Bursts. *arXiv e-prints*, page arXiv:1605.05890, May 2016. [arXiv:1605.05890](#), [\[DOI\]](#), [\[ADS\]](#).
- [62] B. Marcote et al. A repeating fast radio burst source localized to a nearby spiral galaxy. *Nature*, 577(7789):190–194, January 2020. [arXiv:2001.02222](#), [\[DOI\]](#), [\[ADS\]](#).
- [63] K. M. Rajwade et al. First discoveries and localizations of Fast Radio Bursts with MeerTRAP: real-time, commensal MeerKAT survey. *MNRAS*, 514(2):1961–1974, August 2022. [arXiv:2205.14600](#), [\[DOI\]](#), [\[ADS\]](#).
- [64] L. N. Driessen et al. FRB 20210405I: a nearby Fast Radio Burst localized to sub-arcsecond precision with MeerKAT. *MNRAS*, 527(2):3659–3673, January 2024. [arXiv:2302.09787](#), [\[DOI\]](#), [\[ADS\]](#).
- [65] Liam Connor et al. Deep Synoptic Array Science: Two Fast Radio Burst Sources in Massive Galaxy Clusters. *ApJL*, 949(2):L26, June 2023. [arXiv:2302.14788](#), [\[DOI\]](#), [\[ADS\]](#).
- [66] Cherie K. Day, Adam T. Deller, Ryan M. Shannon, Hao Qiu, Keith W. Bannister, Shivani Bhandari, Ron Ekers, Chris Flynn, Clancy W. James, Jean-Pierre Macquart, Elizabeth K. Mahony, Chris J. Phillips, and J. Xavier Prochaska. High time resolution and polarization properties of ASKAP-localized fast radio bursts. *MNRAS*, 497(3):3335–3350, September 2020. [arXiv:2005.13162](#), [\[DOI\]](#), [\[ADS\]](#).
- [67] T. Eftekhari et al. The Massive and Quiescent Elliptical Host Galaxy of the Repeating Fast Radio Burst FRB 20240209A. *ApJL*, 979(2):L22, February 2025. [arXiv:2410.23336](#), [\[DOI\]](#), [\[ADS\]](#).
- [68] Vishwangi Shah et al. A Repeating Fast Radio Burst Source in the Outskirts of a Quiescent Galaxy. *ApJL*, 979(2):L21, February 2025. [arXiv:2410.23374](#), [\[DOI\]](#), [\[ADS\]](#).
- [69] M. Caleb et al. A subarcsec localized fast radio burst with a significant host galaxy dispersion measure contribution. *MNRAS*, 524(2):2064–2077, September 2023. [arXiv:2302.09754](#), [\[DOI\]](#), [\[ADS\]](#).

- [70] Tomas Cassanelli et al. A fast radio burst localized at detection to an edge-on galaxy using very-long-baseline interferometry. *Nature Astronomy*, 8:1429–1442, November 2024. [arXiv:2307.09502](#), [DOI], [ADS].
- [71] Stella Koch Ocker, James M. Cordes, and Shami Chatterjee. Constraining Galaxy Halos from the Dispersion and Scattering of Fast Radio Bursts and Pulsars. *ApJ*, 911(2):102, April 2021. [arXiv:2101.04784](#), [DOI], [ADS].
- [72] Shivani Bhandari, Alexa C. Gordon, Danica R. Scott, Lachlan Marnoch, Navin Sridhar, Pravir Kumar, Clancy W. James, Hao Qiu, Keith W. Bannister, Adam T. Deller, Tarraneh Eftekhari, Wen-fai Fong, Marcin Glowacki, J. Xavier Prochaska, Stuart D. Ryder, Ryan M. Shannon, and Sunil Simha. A Nonrepeating Fast Radio Burst in a Dwarf Host Galaxy. *ApJ*, 948(1):67, May 2023. [arXiv:2211.16790](#), [DOI], [ADS].
- [73] Shivani Bhandari, Keith W. Bannister, Emil Lenc, Hyerin Cho, Ron Ekers, Cherie K. Day, Adam T. Deller, Chris Flynn, Clancy W. James, Jean-Pierre Macquart, Elizabeth K. Mahony, Lachlan Marnoch, Vanessa A. Moss, Chris Phillips, J. Xavier Prochaska, Hao Qiu, Stuart D. Ryder, Ryan M. Shannon, Nicolas Tejos, and O. Ivy Wong. Limits on Precursor and Afterglow Radio Emission from a Fast Radio Burst in a Star-forming Galaxy. *ApJL*, 901(2):L20, October 2020. [arXiv:2008.12488](#), [DOI], [ADS].
- [74] Hao Qiu, Ryan M. Shannon, Wael Farah, Jean-Pierre Macquart, Adam T. Deller, Keith W. Bannister, Clancy W. James, Chris Flynn, Cherie K. Day, Shivani Bhandari, and Tara Murphy. A population analysis of pulse broadening in ASKAP fast radio bursts. *MNRAS*, 497(2):1382–1390, September 2020. [arXiv:2006.16502](#), [DOI], [ADS].
- [75] Stella Koch Ocker, James M. Cordes, Shami Chatterjee, Di Li, Chen-Hui Niu, James W. McKee, Casey J. Law, and Reshma Anna-Thomas. Scattering variability detected from the circumsource medium of FRB 20190520B. *MNRAS*, 519(1):821–830, February 2023. [arXiv:2210.01975](#), [DOI], [ADS].
- [76] K. W. Bannister et al. A single fast radio burst localized to a massive galaxy at cosmological distance. *Science*, 365(6453):565–570, August 2019. [arXiv:1906.11476](#), [DOI], [ADS].
- [77] S. D. Ryder, K. W. Bannister, S. Bhandari, A. T. Deller, R. D. Ekers, M. Glowacki, A. C. Gordon, K. Gourdji, C. W. James, C. D. Kilpatrick, W. Lu, L. Marnoch, V. A. Moss, J. X. Prochaska, H. Qiu, E. M. Sadler, S. Simha, M. W. Sammons, D. R. Scott, N. Tejos, and R. M. Shannon. A luminous fast radio burst that probes the Universe at redshift 1. *Science*, 382(6668):294–299, October 2023. [arXiv:2210.04680](#), [DOI], [ADS].
- [78] Masoud Rafei-Ravandi, Kendrick M. Smith, Dongzi Li, Kiyoshi W. Masui, Alexander Josephy, Matt Dobbs, Dustin Lang, Mohit Bhardwaj, Chitrang Patel, Kevin Bandura, Sabrina Berger, P. J. Boyle, Charanjot Brar, Daniela Breitman, Tomas Cassanelli, Pragya Chawla, Fengqiu Adam Dong, Emmanuel Fonseca, B. M. Gaensler, Utkarsh Giri, Deborah C. Good, Mark Halpern, Jane Kaczmarek, Victoria M. Kaspi, Calvin Leung, Hsiu-Hsien Lin, Juan Mena-Parra, B. W. Meyers, D. Michilli, Moritz Münchmeyer, Cherry Ng, Emily Petroff, Ziggy Pleunis, Mubdi Rahman, Pranav Sanghavi, Paul Scholz, Kaitlyn Shin, Ingrid H. Stairs, Shriharsh P. Tendulkar, Keith Vanderlinde, and Andrew Zwaniga. CHIME/FRB Catalog 1 Results: Statistical Cross-correlations with Large-scale Structure. *ApJ*, 922(1):42, November 2021. [arXiv:2106.04354](#), [DOI], [ADS].
- [79] Kenzie Nimmo, Ziggy Pleunis, Paz Beniamini, Pawan Kumar, Adam E. Lanman, D. Z. Li, Robert Main, Mawson W. Sammons, Shion Andrew, Mohit Bhardwaj, Shami Chatterjee, Alice P. Curtin, Emmanuel Fonseca, B. M. Gaensler, Ronniy C. Joseph, Zarif Kader, Victoria M. Kaspi, Mattias Lazda, Calvin Leung, Kiyoshi W. Masui, Ryan Mckinven, Daniele Michilli, Ayush Pandhi, Aaron B. Pearlman,

- Masoud Rafei-Ravandi, Ketan R. Sand, Kaitlyn Shin, Kendrick Smith, and Ingrid H. Stairs. Magnetospheric origin of a fast radio burst constrained using scintillation. *Nature*, 637(8044):48–51, January 2025. [arXiv:2406.11053](#), [DOI], [ADS].
- [80] Xiang-Lei Chen, Chao-Wei Tsai, Daniel Stern, Christopher D. Bochenek, Shami Chatterjee, Casey Law, Di Li, Chenhui Niu, Yuu Niino, Yi Feng, Pei Wang, Roberto J. Assef, Guodong Li, Sean E. Lake, Gan Luo, and Mai Liao. The Host Galaxy of FRB 20190520B and Its Unique Ionized Gas Distribution. *arXiv e-prints*, page arXiv:2503.01740, March 2025. [arXiv:2503.01740](#), [DOI], [ADS].
- [81] Elizabeth K. Mahony, Ron D. Ekers, Jean-Pierre Macquart, Elaine M. Sadler, Keith W. Bannister, Shivani Bhandari, Chris Flynn, Bärbel S. Koribalski, J. Xavier Prochaska, Stuart D. Ryder, Ryan M. Shannon, Nicolas Tejos, Matthew T. Whiting, and O. I. Wong. A Search for the Host Galaxy of FRB 171020. *ApJL*, 867(1):L10, November 2018. [arXiv:1810.04354](#), [DOI], [ADS].
- [82] Casey J. Law, Kritti Sharma, Vikram Ravi, Ge Chen, Morgan Catha, Liam Connor, Jakob T. Faber, Gregg Hallinan, Charlie Harnach, Greg Hellbourg, Rick Hobbs, David Hodge, Mark Hodges, James W. Lamb, Paul Rasmussen, Myles B. Sherman, Jun Shi, Dana Simard, Reynier Squillace, Sander Weinreb, David P. Woody, and Nitika Yadlapalli Yurk. Deep Synoptic Array Science: First FRB and Host Galaxy Catalog. *ApJ*, 967(1):29, May 2024. [arXiv:2307.03344](#), [DOI], [ADS].
- [83] Mandana Amiri et al. A Catalog of Local Universe Fast Radio Bursts from CHIME/FRB and the KKO Outrigger. *arXiv e-prints*, page arXiv:2502.11217, February 2025. [arXiv:2502.11217](#), [ADS].
- [84] R. M. Shannon et al. The Commensal Real-time ASKAP Fast Transient incoherent-sum survey. *arXiv e-prints*, page arXiv:2408.02083, August 2024. [arXiv:2408.02083](#), [DOI], [ADS].
- [85] Mohit Bhardwaj et al. Host Galaxies for Four Nearby CHIME/FRB Sources and the Local Universe FRB Host Galaxy Population. *ApJL*, 971(2):L51, August 2024. [arXiv:2310.10018](#), [DOI], [ADS].
- [86] Chime/Frb Collaboration and Andersen et al. CHIME/FRB Discovery of 25 Repeating Fast Radio Burst Sources. *ApJ*, 947(2):83, April 2023. [arXiv:2301.08762](#), [DOI], [ADS].
- [87] Daniele Michilli et al. Subarcminute Localization of 13 Repeating Fast Radio Bursts Detected by CHIME/FRB. *ApJ*, 950(2):134, June 2023. [arXiv:2212.11941](#), [DOI], [ADS].
- [88] Vikram Ravi et al. Deep Synoptic Array Science: Discovery of the Host Galaxy of FRB 20220912A. *ApJL*, 949(1):L3, May 2023. [arXiv:2211.09049](#), [DOI], [ADS].
- [89] Vikram Ravi, Casey J. Law, Dongzi Li, Kshitij Aggarwal, Mohit Bhardwaj, Sarah Burke-Spolaor, Liam Connor, T. Joseph W. Lazio, Dana Simard, Jean Somalwar, and Shriharsh P. Tendulkar. The host galaxy and persistent radio counterpart of FRB 20201124A. *MNRAS*, 513(1):982–990, June 2022. [arXiv:2106.09710](#), [DOI], [ADS].
- [90] Adaeze L. Ibik et al. Proposed Host Galaxies of Repeating Fast Radio Burst Sources Detected by CHIME/FRB. *ApJ*, 961(1):99, January 2024. [arXiv:2304.02638](#), [DOI], [ADS].
- [91] Kasper E. Heintz et al. Host Galaxy Properties and Offset Distributions of Fast Radio Bursts: Implications for Their Progenitors. *ApJ*, 903(2):152, November 2020. [arXiv:2009.10747](#), [DOI], [ADS].
- [92] Shivani Bhandari et al. Characterizing the Fast Radio Burst Host Galaxy Population and its Connection to Transients in the Local and Extragalactic Universe. *AJ*, 163(2):69, February 2022. [arXiv:2108.01282](#), [DOI], [ADS].

- [93] Alexa C. Gordon et al. The Demographics, Stellar Populations, and Star Formation Histories of Fast Radio Burst Host Galaxies: Implications for the Progenitors. *ApJ*, 954(1):80, September 2023. [arXiv:2302.05465](#), [DOI], [ADS].
- [94] J. Xavier Prochaska, Jean-Pierre Macquart, Matthew McQuinn, Sunil Simha, Ryan M. Shannon, Cherie K. Day, Lachlan Marnoch, Stuart Ryder, Adam Deller, Keith W. Bannister, Shivani Bhandari, Rongmon Bordoloi, John Bunton, Hyerin Cho, Chris Flynn, Elizabeth K. Mahony, Chris Phillips, Hao Qiu, and Nicolas Tejos. The low density and magnetization of a massive galaxy halo exposed by a fast radio burst. *Science*, 366(6462):231–234, October 2019. [arXiv:1909.11681](#), [DOI], [ADS].
- [95] Casey J. Law, Bryan J. Butler, J. Xavier Prochaska, Barak Zackay, Sarah Burke-Spolaor, Alexandra Mannings, Nicolas Tejos, Alexander Josephy, Bridget Andersen, Pragya Chawla, Kasper E. Heintz, Kshitij Aggarwal, Geoffrey C. Bower, Paul B. Demorest, Charles D. Kilpatrick, T. Joseph W. Lazio, Justin Linford, Ryan Mckinven, Shriharsh Tendulkar, and Sunil Simha. A Distant Fast Radio Burst Associated with Its Host Galaxy by the Very Large Array. *ApJ*, 899(2):161, August 2020. [arXiv:2007.02155](#), [DOI], [ADS].
- [96] V. Ravi, M. Catha, L. D’Addario, S. G. Djorgovski, G. Hallinan, R. Hobbs, J. Kocz, S. R. Kulkarni, J. Shi, H. K. Vedantham, S. Weinreb, and D. P. Woody. A fast radio burst localized to a massive galaxy. *Nature*, 572(7769):352–354, August 2019. [arXiv:1907.01542](#), [DOI], [ADS].
- [97] Alexa C. Gordon, Wen-fai Fong, Sunil Simha, Yuxin Dong, Charles D. Kilpatrick, Adam T. Deller, Stuart D. Ryder, Tarraneh Eftekhari, Marcin Glowacki, Lachlan Marnoch, August R. Muller, Anya E. Nugent, Antonella Palmese, J. Xavier Prochaska, Marc Rafelski, Ryan M. Shannon, and Nicolas Tejos. A Fast Radio Burst in a Compact Galaxy Group at $z \sim 1$. *arXiv e-prints*, page arXiv:2311.10815, November 2023. [arXiv:2311.10815](#), [DOI], [ADS].

List of FRBs

FRB	z	DM_{obs}	DM_{ISM} (NE2001)	DM_{ISM} (YMW2017)	References
FRB20200120E	0.0008	87.77	30	19.54	[56]
FRB20181030A	0.0039	103.5	40	32	[55]
FRB20171020A	0.00867	114.1	38	26	[81]
FRB20220319D	0.0112	110.98	133.3	210.96	[82]
FRB20231229A	0.0190	198.5	58.12	51.78	[83]
FRB20240210A	0.0238	283.75	31	17.90	[84]
FRB20181220A	0.027	209.4	125.8	122.1	[85]
FRB20231230A	0.0298	131.4	61.51	83.24	[83]
FRB20181223C	0.03024	112.51	19.91	19.1	[85]
FRB20190425A	0.03122	128.16	48.75	38.86	[85]
FRB20180916B	0.0337	348.76	200	324.95	[62]
FRB20230718A	0.035	477	396	467.25	[84]
FRB20240201A	0.0427	374.5	38	29.15	[84]
FRB20220207C	0.0430	262.38	79.3	83.27	[82]
FRB20211127I	0.0469	234.83	42.5	31.46	[12]
FRB20201123A	0.0507	433.55	251.93	162.4	[63]
FRB20230926A	0.0553	222.8	52.69	43.71	[83]
FRB20200223B	0.06024	202.268	46	37	[86]
FRB20190303A	0.064	222.4	26	21.79	[87]
FRB20231204A	0.0644	221.0	29.73	21.79	[83]
FRB20231206A	0.0659	457.7	59.13	59.29	[83]
FRB20210405I	0.066	565.17	516.1	348.7	[64]
FRB20180814	0.068	189.4	87	108	[87]
FRB20231120A	0.07	438.9	43.8	36.22	[1]
FRB20231005A	0.0713	189.4	33.37	28.79	[83]
FRB20190418A	0.07132	184.5	70.1	85.6	[85]
FRB20211212A	0.0715	206.0	27.1	27.46	[12]
FRB20231123A	0.0729	302.1	89.76	136.89	[83]
FRB20220912A	0.0771	219.46	115	122.24	[88]
FRB20231011A	0.0783	186.3	70.36	65.70	[83]
FRB20220509G	0.0894	269.53	55.2	52.06	[82]
FRB20230124	0.0940	590.6	38.5	31.77	[45],[1]
FRB20201124A	0.098	413	123	196.67	[89]
FRB20230708A	0.105	411.51	50	43.90	[84]
FRB20231223C	0.1059	165.8	47.9	38.64	[83]
FRB20191106C	0.10775	333.4	25	21	[90]
FRB20231128A	0.1079	331.6	25.05	20.54	[83]
FRB20230222B	0.11	187.8	27.7	26.4	[83]
FRB20231201A	0.1119	169.4	70.03	74.72	[83]
FRB20220914A	0.1139	631.28	55.2	51.11	[82]

FRB	z	DM_{obs}	$DM_{\text{ISM}} (\text{NE2001})$	$DM_{\text{ISM}} (\text{YMW2017})$	References
FRB20190608B	0.1178	339	37	26.62	[9]
FRB20230703A	0.1184	291.3	26.97	20.67	[83]
FRB20240213A	0.1185	357.4	40.1	32.10	[1]
FRB202030222A	0.1223	706.1	134.13	188.14	[83]
FRB20190110C	0.1224	221.961	35.66	28.96	[90]
FRB20230628A	0.1265	345.15	39.1	33.36	[45],[1]
FRB20240310A	0.127	601.8	36	19.83	[84]
FRB20210807D	0.1293	251.9	121.2	93.63	[12]
FRB20240209A	0.1384	176.49	55.5	52.2	[68]
FRB20210410D	0.1415	578.78	56.2	42.2	[69]
FRB20230203A	0.1464	420.1	36.29	22.98	[83]
FRB20231226A	0.1569	329.9	145	26.72	[84]
FRB20230526A	0.157	316.4	50	21.88	[84]
FRB20220920A	0.158	314.99	40.3	30.83	[82]
FRB20200430A	0.1608	380.25	27	26.08	[91]
FRB20210603A	0.177	500.15	40	30.79	[70]
FRB20230311A	0.1918	364.3	92.39	115.68	[83]
FRB20220725A	0.1926	290.4	31	61.24	[84]
FRB20221106A	0.2044	343.8	35	31.85	[84]
FRB20240215A	0.21	549.5	48.0	42.79	[1]
FRB20230730A	0.2115	312.5	85.18	97.29	[83]
FRB20210117A	0.214	729.0	34.0	23.0	[72]
FRB20221027A	0.229	452.5	47.2	40.59	[1]
FRB20191001A	0.234	506.92	44.7	31.08	[91]
FRB20190714A	0.2365	504.13	38	31.16	[91]
FRB20221101B	0.2395	490.7	131.2	193.36	[45],[1]
FRB20220825A	0.2414	651.24	79.7	86.98	[82]
FRB20191228A	0.2432	297.5	33	19.93	[92]
FRB20231017A	0.2450	344.2	64.55	55.64	[83]
FRB20221113A	0.2505	411.4	91.7	115.40	[45],[1]
FRB20220307B	0.2507	499.15	128.2	186.98	[45],[1]
FRB20220831A	0.262	1146.25	126.7	188	[1]
FRB20231123B	0.2625	396.7	40.2	33.81	[45],[1]
FRB20230307A	0.2710	608.9	37.6	29.47	[45],[1]
FRB20221116A	0.2764	640.6	132.3	196.18	[1]
FRB20220105A	0.2785	583	22	20.64	[84]
FRB20210320C	0.2796	384.8	42.2	30.39	[12]
FRB20221012A	0.2846	441.08	54.4	50.55	[82]
FRB20240229A	0.287	491.15	37.9	29.52	[1]
FRB20190102C	0.2913	363.6	57.3	43.38	[9]
FRB20220506D	0.3004	396.97	89.1	72.83	[82]
FRB20230501A	0.3010	532.5	125.6	180.17	[45],[1]

FRB	z	DM _{obs}	DM _{ISM} (NE2001)	DM _{ISM} (YMW2017)	References
FRB20180924B	0.3214	361.42	40.5	27.66	[76]
FRB20231025B	0.3238	368.7	48.67	43.36	[83]
FRB20230626A	0.3270	451.2	39.2	32.51	[45],[1]
FRB20180301A	0.3304	536	152	253.96	[92]
FRB20231220A	0.3355	491.2	49.9	44.54	[1]
FRB20211203C	0.3439	635.0	63.4	48.37	[93]
FRB20220208A	0.3510	437.0	101.6	128.80	[45],[1]
FRB20220726A	0.3610	686.55	89.5	111.40	[45],[1]
FRB20230902A	0.3619	440.1	34	25.62	[84]
FRB20200906A	0.3688	577.8	36	37.87	[92]
FRB20240119A	0.37	483.1	37.9	30.98	[1]
FRB20220330D	0.3714	468.1	38.6	30.09	[45],[1]
FRB20190611B	0.3778	321.4	57.8	43.67	[91]
FRB20220501C	0.381	449.5	31	14	[84]
FRB20220204A	0.4	612.2	50.7	46.03	[1]
FRB20230712A	0.4525	586.96	39.2	30.93	[45], [1]
FRB20181112A	0.4755	589.27	42	29.03	[94]
FRB20220310F	0.4779	462.24	45.4	39.51	[82]
FRB20220918A	0.491	656.8	41	28.85	[84]
FRB20190711A	0.5220	593.1	56.4	42.62	[91]
FRB20230216A	0.5310	828.0	38.5	27.05	[45], [1]
FRB20230814A	0.5535	696.4	104.9	134.83	[1]
FRB20221219A	0.5540	706.7	44.4	38.60	[45], [1]
FRB20190614D	0.60	959.2	83.5	108.72	[95]
FRB20220418A	0.6220	623.25	37.6	29.54	[82]
FRB20190523A	0.6600	760.8	37	29.88	[96]
FRB20240123A	0.968	1462.0	90.3	112.98	[1]
FRB20221029A	0.9750	1391.05	43.9	36.4	[1, 45]
FRB20220610A	1.016	1458.1	30.9	13.58	[97]

Table 2: List of 110 FRBs used in this work along side their redshifts, total observed DM, ISM contribution using NE2001 and YMW2017 model and their published references.

A Sample of FRBs

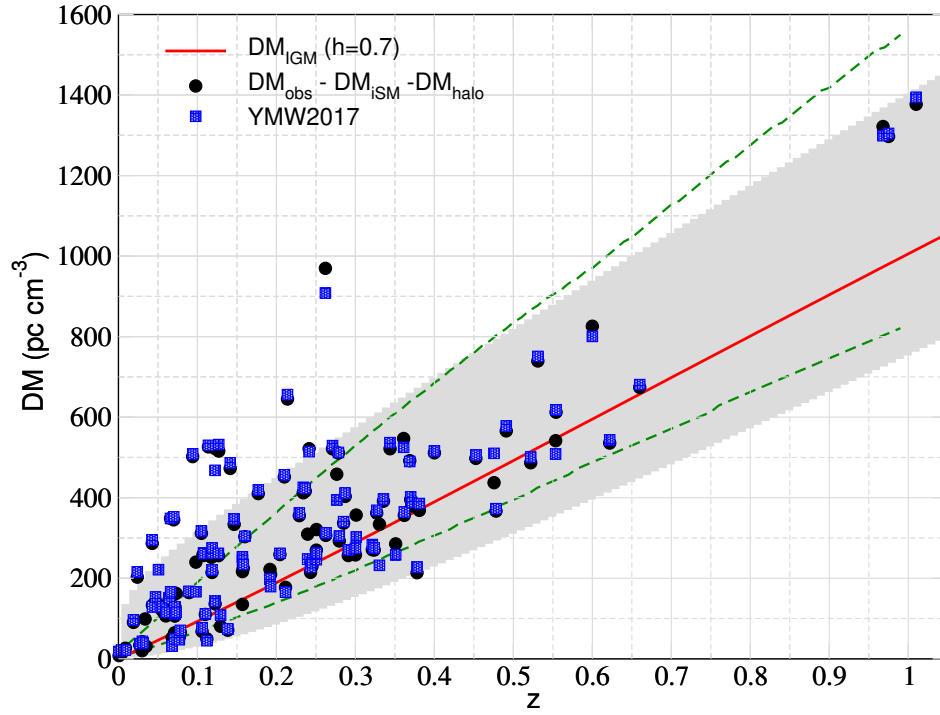


Figure 6: Dispersion measure of our sample of 110 FRBs after subtracting ISM and halo contribution from observed DM. We compare it to our fiducial IGM model with $h = 0.7$. The shaded grey region shows the 1σ region due to scatter in IGM (Eq. 3.3). We also show an estimate of the 68 percent confidence interval of DM_{IGM} distribution obtained from IllustrisTNG simulation [38] in green dashed lines.